An α-Helical Burst in the src SH3 Folding Pathway

Jinsong Li,[‡] Masaji Shinjo,[‡] Yoshitaka Matsumura,[‡] Masayuki Morita,[§] David Baker,[||] Masamichi Ikeguchi,[⊥] and Hiroshi Kihara*,[‡]

Departments of Physics and Molecular Biology, Kansai Medical University, 18-89 Uyama-Higashi, Hirakata 573-1136, Japan, Department of Biochemistry, University of Washington, Seattle, Washington 98195, and Department of Bioinformatics, Soka University, Hachioji, Japan

Received September 1, 2006; Revised Manuscript Received January 27, 2007

ABSTRACT: Src SH3 is a small all-β-sheet protein composed of a single domain. We studied the folding behavior of src SH3 at various conditions by circular dichroism (CD), fluorescence, and X-ray solution scattering methods. On the src SH3 folding pathway, an α-helix-rich intermediate appeared not only at subzero temperatures but also above 0 °C. The fraction of α-helix in the kinetically observed intermediate is ca. 26% based on the kinetic CD experiment. X-ray solution scattering revealed that the intermediate was compact but not fully packed. The analysis of CD implies that the amplitude of the burst phase is proportional to the helical fraction calculated according to the helix−coil transition theory. This strongly suggests that the initial folding core is formed by the collapse of much less stably existing α-helices.

The biological function of globular proteins is determined by their native structure. Therefore, understanding how proteins fold into their compact forms is a central problem in modern structure biology (*1*). In the past few years, we have been studying the refolding process of proteins such as ubiquitin (*2*, *3*) and bovine β-lactoglobulin (BLG)[1] (*4*) at low temperatures. They are mainly composed of β-structures.

It appears that several such proteins form α-helical intermediates before acquiring their native β-sheet structure. BLG has been thoroughly studied from experimental and theoretical points of view (*5*−*8*). We have reported how BLG formed an α-helix-rich intermediate and then converted to its native-like structure at a temperature as low as −28 °C. This indicated that the α-helix-rich folding core was formed in the folding process of the β-structure-rich protein (*4*). We have also studied another small β-structure-rich protein (76 amino acids), ubiquitin. It also shows a non-native helix formation at its early stage, the rate of which depends on the temperature and the viscosity of the solution, but the amplitude of the CD value of the intermediate did not depend on them (*3*). We therefore pose the question: Does the non-native helix formed at the early stage of the β-structure-rich protein folding process appear in general?

BLG belongs to the UDβ (up and down β-barrel) family. Nishikawa and co-workers reported that the helical content of BLG in trifluoroethanol was correlated with the helical content predicted by the secondary structure prediction program, suggesting that the helical structure of BLG in trifluoroethanol is mainly stabilized by local interaction (*9*). In addition, Chikenji et al. reported that the free energy analysis shows a strong probability of forming α-helix-rich intermediates in the BLG folding process (*10*). Secondary structure prediction analysis of BLG shows a high helix propensity in sequence as discussed below. Therefore, it could have been argued that an α-helix-rich intermediate appears only in the folding process of β-lactoglobulin as an exceptional case due to a consequence of high helix propensity.

Src homology domain 3 (SH3) is a small protein (50−70 amino acids) that is involved in the signal transduction in the cell. SH3 domains comprise a huge protein family (*11*). They take the same fold topology: two small orthogonal three-stranded β-sheets with an associated irregular two-stranded sheet packing against each other in a sandwich structure (*12*). Using several secondary structure prediction methods, we find that src SH3 has much lower helix propensity than BLG (Figure 1). Therefore, src SH3 is not a type of UDβ protein. Qin et al. (*13*) studied the folding process of src SH3 at −20 °C in the presence of 45% ethylene glycol (EGOH) as antifreeze. Surprisingly, they also found a large α-helix burst within the dead time of the stopped-flow (SF) apparatus (6 ms). This result indicated that even the all-β-structure proteins can form an α-helix-rich conformation in its folding process, though the experiment was done at subzero temperatures and with 45% EGOH as antifreeze. Chikenji et al. explored the folding free energy of src SH3 under physiological conditions. They also found the large amount α-helix formed at the early stage of src SH3 folding (*14*).

To bring the folding condition closer to physiological values, in the present paper, we investigated the folding

* To whom correspondence should be addressed. Phone: +81-72-856-2121. Fax: +81-72-850-0733. E-mail: kihara@makino.kmu.ac.jp.
[‡] Department of Physics, Kansai Medical University.
[§] Department of Molecular Biology, Kansai Medical University.
[||] University of Washington.
[⊥] Soka University.

[1] Abbreviations: SH3, Src homology domain 3; CD, circular dichroism; EGOH, ethylene glycol; GuHCl, guanidine hydrochloride; R_g, radius of gyration; I_0, zero angle intensity; UV, ultraviolet; SF, stopped flow; PBS, sodium phosphate buffer; SF-XS, stopped-flow X-ray scattering; BLG, bovine β-lactoglobulin; ELG, equine β-lactoglobulin; Mb, myoglobin.

10.1021/bi0618262 CCC: $37.00
Published on Web 04/07/2007

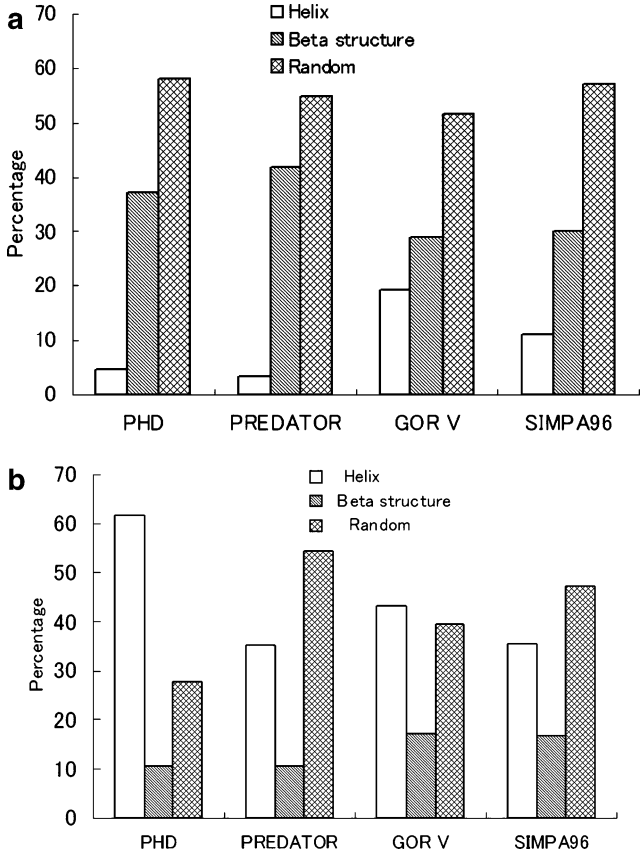

FIGURE 1: Predicted secondary structures of BLG and src SH3 by PHD, predator, GOR V, and SIMPA96: (a) src SH3; (b) BLG.

process of src SH3 in aqueous buffer above 0 °C with multiple probes (CD, fluorescence, and X-ray solution scattering). We observed an α-helical-rich intermediate on the src SH3 folding pathway at 4 °C. The SH3 homology protein, the Fyn SH3 domain, showed similar folding behavior.

MATERIALS AND METHODS

Protein Expression and Purification. src SH3 was expressed in *Escherichia coli* BL21(DE3) pLysS (Novagen) from the plasmid src SH3-pET 15b (*15*). Cells were lysed using a combined sonic and freeze/thraw method after expression and then centrifuged by 12000*g* for 30 min. After the single step Zn^{2+} affinity column (Pharmachia), the follow-through was further separated by gel filtration, Sephacryl S-100 (Pharmacia). The His tag was not cut in the present study. Tris−tricine electrophoresis (*16*) confirmed that the molecular weight of the protein was ca. 8700. ESI mass spectroscopy proved that the molecular weight is 8767, which is exactly the same as that calculated from the amino acid sequence. The purity of the protein is better than 99%, judging from the mass spectroscopy. All experiments were performed in 50 mM sodium phosphate buffer (PBS) at pH 3.0, unless otherwise stated. The concentration of SH3 was determined spectrophotometrically by using the extinction coefficient $\epsilon_{280} = 16500\ M^{-1}\ cm^{-1}$ (*17*). The plasmid for Fyn* W120F was obtained by single point mutation of the original Fyn plasmid (constructed by Davidson and provided by the Gruebele group) using site-directed mutagenesis (Stratagene). Fyn* was also expressed in *E. coli* (BL21). After IPTG induction and 4−6 h of growth at 37 °C, cells were harvested and lysed in 6 M GuHCl, 100 mM NaH_2PO_4, 10 mM Tris-HCl, 10 mM imidazole, 1 mM phenylmethanesulfonyl fluoride, and 1 mM benzamidine at pH 8.0. Purification was carried out by a batch procedure in the same buffer using Ni-NTA−agarose resin (Pharmacia). Purified proteins were eluted with 3 M GuHCl, 100 mM EDTA, 50 mM NaH_2PO_4,1 mM PMSF, and 1 mM benzamidine at pH 6.0 and were refolded by a 10 times diluted solution into 50 mM PBS at pH 6.0. The protein solution was concentrated by a VIVASpin filter membrane (MW 3500), and then the protein solution was further separated by gel filtration, Sephacryl S-100 (Pharmacia). Purity was checked by Tris−tricine electrophoresis. For storage, samples were lyophilized and kept at −20 °C after dialysis against distilled water. The concentration of Fyn SH3 was determined by using the extinction coefficient $\epsilon_{280} = 12500\ M^{-1}\ cm^{-1}$ (*17*).

CD Measurements. All CD measurements were performed in the far-UV region (200−250 nm) with the spectropolarimeter (Unisoku, Japan) to monitor secondary structures (*18*, *19*). In this paper, the units of θ are in deg·cm^2·dmol^{-1}, unless otherwise stated.

Measurements in Equilibrium. The sample was prepared in 50 mM PBS at the appropriate pH with various concentrations of GuHCl, respectively. The final concentration of the protein was kept at 50 μM. The temperature was kept constant by a water bath surrounding the cuvette during measurements. All samples were prepared freshly before use. A cuvette of 1 mm path length was used for all measurements.

Kinetic CD Measurements. Kinetic SH3 refolding experiments were performed as described elsewhere (*2*−*4*). The refolding process of src SH3 was initiated by SF. Six volumes of buffer solution was mixed with one volume of unfolded protein solution in 5 M GuHCl, thus by 7-fold dilution of GuHCl, i.e., from 5 to 0.71 M. The refolding process was monitored with CD at 217, 220, 222, 225, 230, 235, and 240 nm. The calibrated dead time of the SF is 6 ms (unpublished result). The final concentration of the protein was 50 μM. The CD signal was traced with multiple accumulations until getting a good signal to noise ratio. The amplitude of the burst phase (the phase which is finished within the dead time of the SF) was obtained as the difference of the first point and the level of the initial value at 0 s, where the initial value was obtained by mixing the protein in the unfolded solution with the unfolded buffer. The temperature was kept at 4 °C, unless otherwise stated.

Fluorescence Measurements in Equilibrium. Tryptophan emission fluorescence measurements were carried out using an F-3000 fluorescence spectrophotometer (Hitachi) with a cuvette of 1 cm light path. The excitation wavelength was 295 nm to eliminate the nonspecific emission of tyrosine. The tryptophan emission fluorescence spectra were collected from 320 to 400 nm.

Kinetic Fluorescence Measurements. The SH3 refolding process was also monitored by the SF-fluorescence method. The SF used was the same apparatus used for kinetic CD measurements. Fluorescence was monitored with a specially designed optical fiber of less than 1 mm thickness, which was inserted into the observation cell of the CD from the above. Fluorescence was excited at 295 nm and integrated at wavelengths above 325 nm with a cutoff filter. The signal was traced with 10−20 times accumulation to get a good

Table 1: Thermodynamic Parameters of src SH3 Unfolding against GuHCl

pH	temp (°C)	method	midpoint	*m* [kJ/(mol M)]	Δ*G* (kJ/mol)
3.0	4	CD	2.1	5.1	10.8
		fluorescence	2.1	5.0	10.6
		SAXS	2.1	5.4	11.3
		Fl-SF[a]		1.6,[b] 2.1[c]	6.8
6.0	4	CD	2.74	6.2	17.3

[a] Fl-SF is fluorescence combined with SF. [b] m_f at low GuHCl concentration (*1*). [c] m_u at high GuHCl concentration (*1*).

Table 2: Folding Rates at Various Conditions

protein	buffer conditions	temp (°C)	probe	rate constant (s^{-1})
src SH3	pH 3.0, aqueous	4	fluorescence	0.9
		4	CD	0.9
		4	SAXS	0.94
		20	fluorescence	2.7
	pH 6.0, aqueous	4	fluorescence	3.15
		4	CD	5.5
		20	fluorescence	17.7
		20	CD	20.3
	pH 3.0, 45% EGOH−55% H_2O	4	CD	1.06
		4	fluorescence	1.045
		−10	fluorescence	0.28
		−20	CD	0.09
		−20	fluorescence	0.093
Fyn SH3	pH 6.0, aqueous	4	CD	76.5
	pH 6.0, 45% EGOH−55% H_2O	−20	CD	1.1, 32

signal to noise ratio. The SH3 was unfolded in 50 mM PBS at pH 3.0 in the presence of 5.0 M GuHCl. The refolding process was initiated by 7-fold dilution of GuHCl, i.e., from 5 to 0.71 M. The final protein concentration was 50 μM.

SAXS Measurements. X-ray solution scattering measurements (SAXS) were performed at beamline 15A of the Photon Factory at KEK (Tsukuba, Japan) (*20*, *21*). The X-ray wavelength was $\lambda = 1.504$ Å with the CCD detector for both kinetic and static measurements (*22*, *23*). To get a good signal to noise ratio, we used a high concentration of SH3, 4 mg/mL at static and 2 mg/mL at kinetic measurements. All measurements were performed at 4 °C. Helium gas was flowed in and around the observation cell in order to prevent frost from forming on the window. X-ray scattering data were taken both on protein solutions and on the corresponding buffers. The scattering data of the buffer were subtracted from those of the protein solution. X-ray scattering data were analyzed by Guinier analysis, assuming an exponential dependence of the scattering intensity on h^2, where $h = 4\pi \sin\theta/\lambda$ and θ is half of the scattering angle (*24*). The linear Guinier region was selected to obtain a radius of gyration (R_g) and zero angle intensity (I_0) in the region of $h \leq 0.05$, where the value of $R_g h$ is less than 1.

For static experiments, the exposure time of the X-ray beam was from 50 to 100 s, depending on the concentration of GuHCl.

For kinetic measurements, the SF apparatus, used in kinetic CD and fluorescence, was also used with another observation cell of 50 μm sapphire window. To get a good signal to noise ratio, the data were accumulated 200 times.

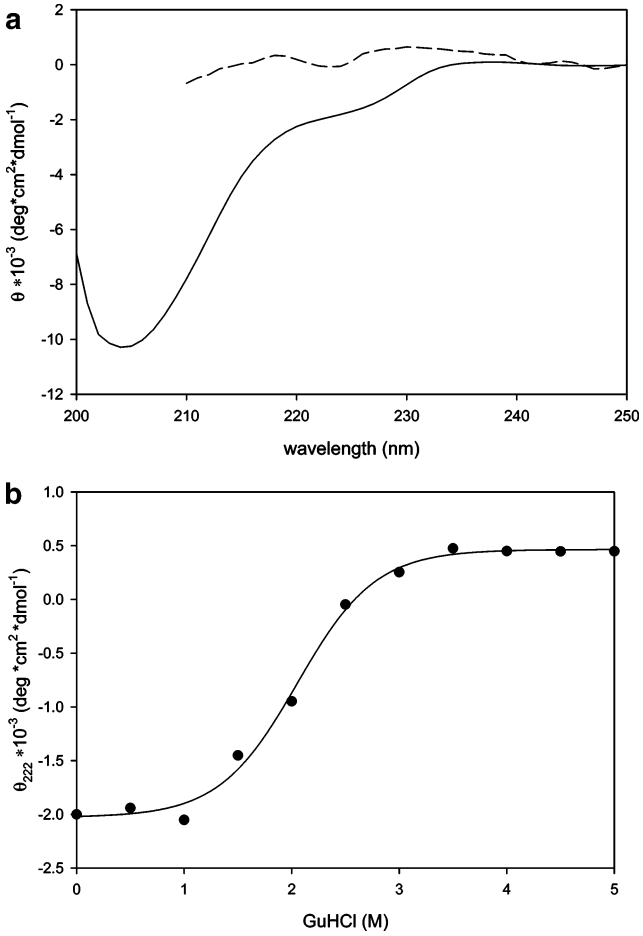

FIGURE 2: CD measurements of src SH3 at various GuHCl concentrations. (a) CD spectra of native and unfolded src SH3 at 4 °C in 50 mM PBS at pH 3.0 (solid line, 0 M GuHCl; dashed line, 5 M GuHCl). (b) CD of src SH3 at 222 nm as a function of GuHCl concentration. The curve is the fit to the experimental data using the simple two-state model as a function of GuHCl. The midpoint of the denaturation is 2.1 M.

RESULTS

Measurements of src SH3 at equilibrium and kinetics were performed with CD at the far-UV region, fluorescence, and X-ray solution scattering at various conditions. As the experiments were carried out with various conditions, we tabulated the static and kinetic experimental conditions in Tables 1 and 2, respectively.

Equilibrium Measurements at pH 3.0 and at 4 °C. (A) Circular Dichroism (CD). GuHCl-induced unfolding transitions of src SH3 were monitored by far-UV CD spectropolarimeter at wavelengths from 200 to 250 nm. At low GuHCl concentration (<1 M), the src SH3 shows a typical β-structure spectrum (Figure 2a). The [θ] at 222 nm is ca. −2000. The smoothed CD spectra at high GuHCl concentration (>3 M) indicate that the secondary structure was totally unfolded (Figure 2a). The plots of θ at 222 nm vs GuHCl concentration show that the protein lost its secondary structure with the increase of the concentration of GuHCl (Figure 2b). The native state protein has −2000 ellipticities at 222 nm. The CD ellipticity value increased to 350 when the protein was totally unfolded in 5 M GuHCl. The nonlinear least-squares fitting gives the characteristic S-shape of the denaturation curves with the midpoint at about 2.1 M.

The GuHCl-induced unfolding curve (Figure 2b) was analyzed according to a two-state folding mechanism. At the two-state model, the free energy of activation for unfolding at any GuHCl concentration, $\Delta G(\mathrm{D})$, is derived as $\Delta G(\mathrm{D}) = \Delta G_{\mathrm{H_2O}} - m[\mathrm{D}]$, where m is the slope, [D] is the denaturant concentration, and $\Delta G_{\mathrm{H_2O}}$ is the free energy of activation for unfolding in water (*1*). The obtained midpoint, m, and $\Delta G_{\mathrm{H_2O}}$ are tabulated in Table 1.

(B) Fluorescence. Fluorescence emission increased significantly with the increase of GuHCl concentration and is accompanied by a 6 nm red shift, reflecting the increase of the exposure of the Trp residue to the solvent (data not shown). Secondary structures as well as tertiary structures were completely disrupted above 3 M GuHCl, judging from the CD spectrum and the intensity ratio of 340 nm/370 nm of fluorescence (data not shown). The GuHCl-induced unfolding curve was also measured by fluorescence, and the data were analyzed according to a two-state folding mechanism. The derived midpoint, m, and $\Delta G_{\mathrm{H_2O}}$ are also tabulated in Table 1.

(C) X-ray Solution Scattering. X-ray scattering experiments of src SH3 were performed at pH 3.0 and 4 °C at various GuHCl concentrations. R_g values of src SH3 were obtained from Guinier analysis at each GuHCl concentration. The typical Guinier plots at 0 and 5 M GuHCl are shown in Figure 3a, and the R_g values thus calculated are plotted against GuHCl concentration in Figure 3c. As seen in Figure 3c, R_g is constant around 14.6 Å at GuHCl lower than 1.5 M and 26.7 Å at GuHCl higher than 3 M with the midpoint at 2.1 M. The derived m and $\Delta G_{\mathrm{H_2O}}$ are tabulated in Table 1. Kratky plots were also obtained at each GuHCl concentration (Figure 3b). Kratky plots show a peak at GuHCl lower than 1.5 M, whereas the peak disappeared at GuHCl higher than 2.5 M. These results indicate that the src SH3 takes the compact native conformation at GuHCl lower than 1.5 M and takes the expanded unfolding state at GuHCl higher than 3 M (*25*). This result is consistent with those obtained from CD and fluorescence.

R_g, which was calculated with the program of SAXS-MD written by Kojima (*26*) based on its crystal structure, was 14.3 Å, slightly smaller than that experimentally obtained at 0 M GuHCl.

All of the experiments with three probes gave essentially consistent unfolding transitions.

Equilibrium Measurements at pH 6.0 and at 4 °C. GuHCl titration of src SH3 was also performed in 50 mM PBS at pH 6.0 and at 4 °C (Figure 9). The CD spectrum at pH 6.0 is the same as at pH 3.0, indicating the src SH3 took the same structure at pH 3.0 and 6.0. The same fitting method was also used to analyze the experimental data at pH 6.0. Midpoint and thermodynamic parameters were thus obtained and shown in Table 1. The midpoint at pH 6.0 was 2.76, whereas that at pH 3.0 was 2.1, indicating the protein is more stable at pH 6.0 than at pH 3.0.

Kinetic Measurements of src SH3 at pH 3.0. The refolding of src SH3 was performed by mixing the denatured protein in 5 M GuHCl with the buffer of six times larger volume, thus getting 0.7 M GuHCl as the final solvent. The refolding reaction was kinetically monitored by CD, fluorescence, and X-ray solution scattering at 4 °C (Figures 4, 6, and 8). SF-CD and SF-fluorescence were also performed at 4 °C and −20 °C in the presence of 45% EGOH as antifreeze.

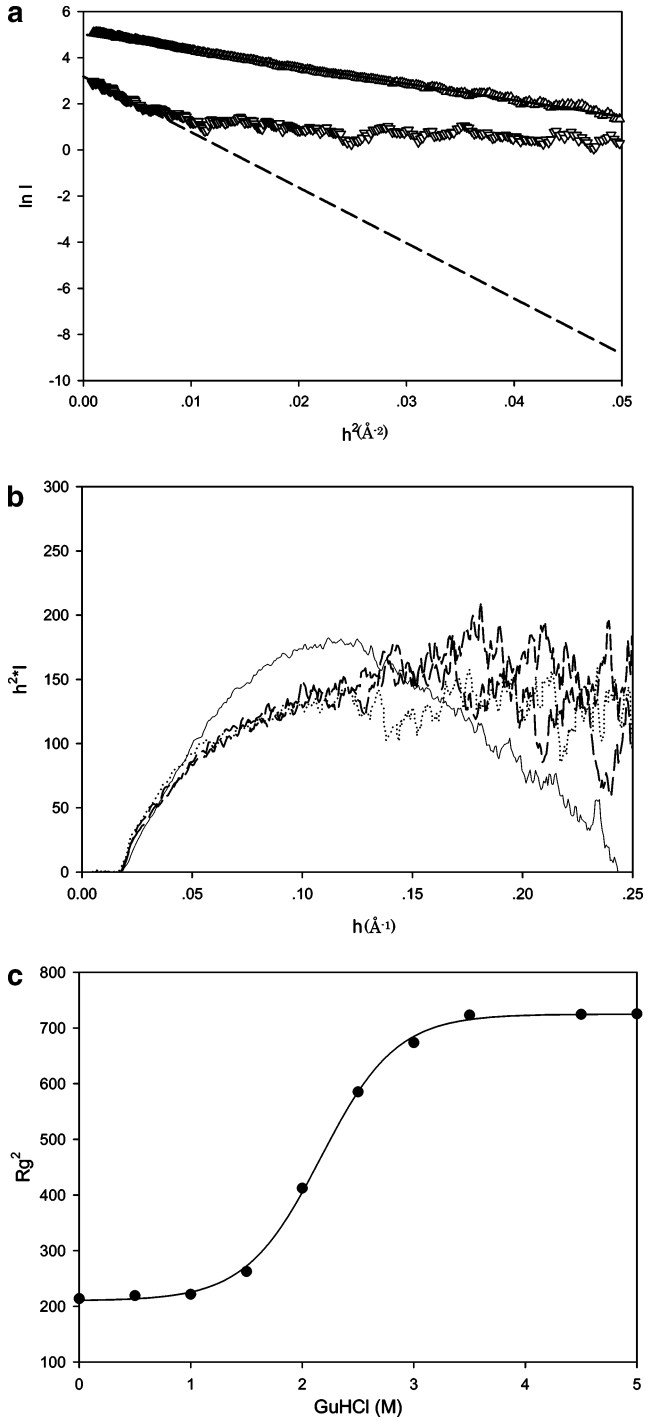

FIGURE 3: X-ray solution scattering of GuHCl-induced unfolding of src SH3 at 4 °C in 50 mM PBS at pH 3.0. (a) Guinier plot of the native and unfolded src SH3 (△, 0 M GuHCl; ▽, 5 M GuHCl). (b) Kratky plot of src SH3 with 0 M (solid line), 2 M (long dashed line), 2.5 M (middle dashed line), and 5 M (dotted line) GuHCl, respectively. From the figure, it is found that the conformation of src SH3 was changed with the increase of GuHCl concentration, and the unfolded protein was dominant in GuHCl concentration higher than 3 M. (c) R_g^2 of src SH3 as a function of GuHCl concentration.

(A) Kinetic CD. CD-SF was used to study the refolding process of src SH3 at different conditions, as shown in Figure 4. The secondary structure conformation change was determined by the ellipticity at 222 nm. All of them can be clearly distinguished by two phases during the refolding process. At 4 °C, the CD signal first dropped down to −8000

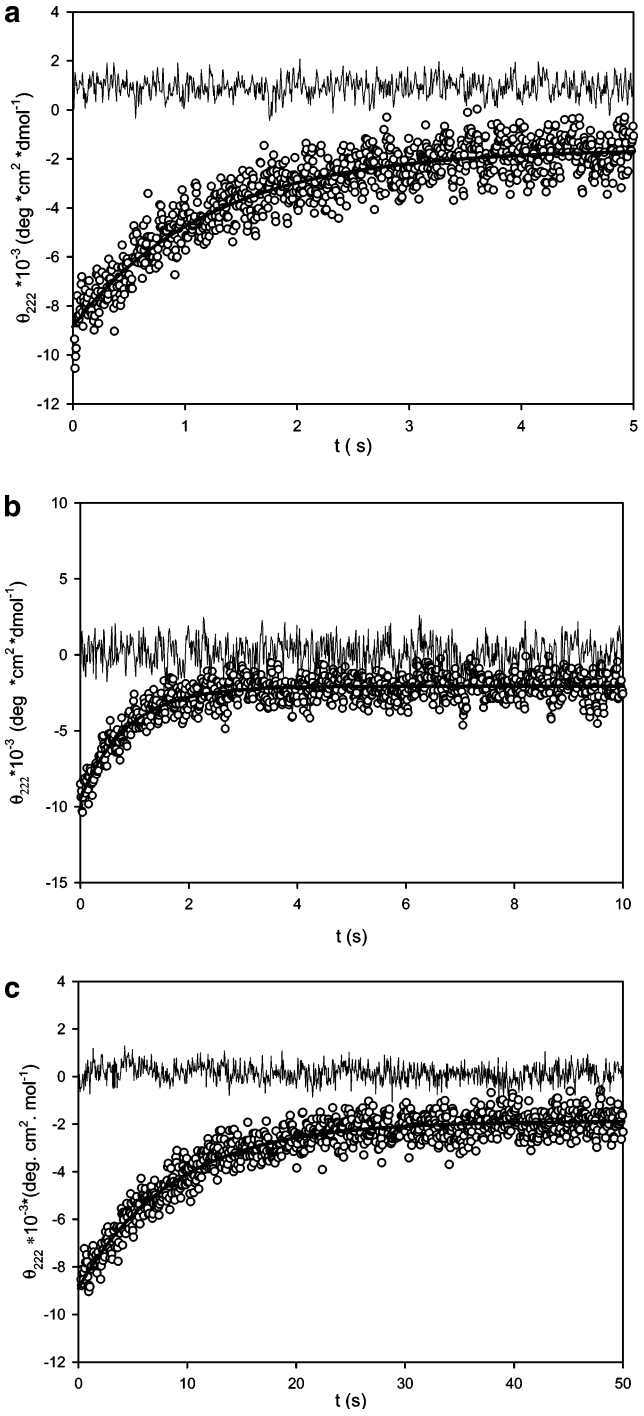

FIGURE 4: CD-SF-monitored refolding of src SH3 in the acidic buffer (pH 3.0). GuHCl jump from 5 to 0.71 M, monitored at 222 nm. The black line is the initial signal. The open circle line is the monitored refolding process. The smoothed solid curve is the simulated refolding signal as a single exponential. (a) In the absence of EGOH at 4 °C. (b) In the presence of 45% EGOH at 4 °C. (c) In the presence of 45% EGOH at −20 °C.

within the dead time of the SF apparatus, which we call the burst phase. The CD signal then slowly increased to −2000 (the value of the native state of src SH3) with a rate constant of 0.9 ± 0.1 s^{-1}. The slowly increased phase was fitted with a single exponential decay. Its amplitude corresponds to about 76% of the burst. The initial level, obtained by mixing the protein solution with unfolding buffer (5 M GuHCl), is ca. 500 by linear fitting of the data. It is very close to the value of unfolding which we observed at the static experiments at 222 nm. The huge burst signal of SF-CD indicated that the intermediate has a large amount of α-helix as discussed below.

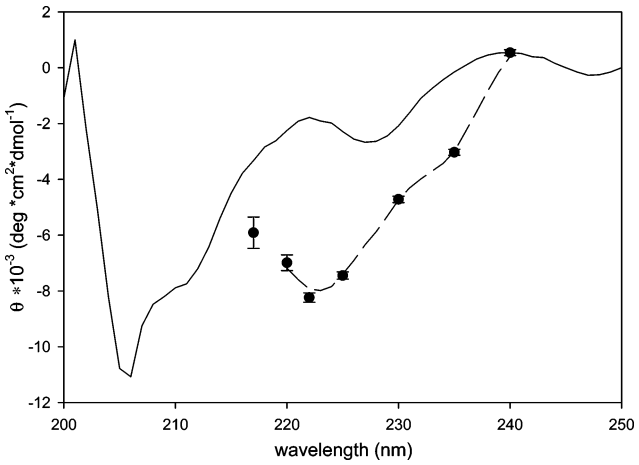

FIGURE 5: Transient CD spectra obtained by CD-SF from 217 to 240 nm at 4 °C in 50 mM PBS at pH 3.0. Dots with error bars are amplitudes of the burst phase. The solid curve is the CD spectrum of the refolded src SH3 taken 10 min after mixing. The broken line is the transient CD spectra calculated by the CONTIN program.

To characterize the transient intermediate in more detail, we measured the burst phase amplitude by SF-CD from 217 to 240 nm at 4 °C. All refolding data were fitted as a single exponential decay. Figure 4 shows the CD spectrum of the transient intermediate and the static measurement of src SH3 10 min after initiating the refolding. The initial level at each wavelength was also compared with the static measurement. At wavelengths below 215 nm, the data were too noisy to be fitted, due to the strong absorbance of GuHCl in the short wavelength region. The transient fraction of the α-helix and *β*-structure was calculated according to the program of CONTIN developed by Provencher (*27*). Its fitting curve was also shown in Figure 5. The estimated fraction of α-helix is 26%. The fraction of α-helix was also calculated with the assumption of coexistence of the helix ($\theta_{222} = -42500$ deg·cm^2·dmol^{-1}) and random coil ($\theta_{222} = 640$ deg·cm^2·dmol^{-1}) (*28*, *29*), giving the fraction of the helix as 21%. These two values are in good agreement, demonstrating the existence of the α-helix at the intermediate state.

(B) Kinetic Fluorescence. The refolding reaction was also monitored by SF tryptophan fluorescence at pH3.0 at various conditions (20 and 4 °C in the absence of EGOH and 4 and −20 °C in the presence of 45% EGOH). In Figure 6, a trace was shown at 4 °C in the absence of EGOH. In all cases, we observed a burst phase and the subsequent resolvable single exponential decay. Obtained rate constants are tabulated in Table 2 as well as in kinetic CD measurements. They are in fairly good agreement at each condition, whereas the burst amplitude is more or less the same at all conditions.

In Figure 7, apparent rate constants (k_{obs}) are plotted as a function of GuHCl concentration. Both unfolding rates at high concentrations of GuHCl and folding rates at low concentrations of GuHCl can be fitted by a linear relation, respectively (*1*). Data were analyzed according to Grantcharova and Baker (*15*). Obtained slopes and ΔG are tabulated in Table 1.

(C) Kinetic X-ray Solution Scattering. To monitor directly the molecular compaction process in protein folding, the

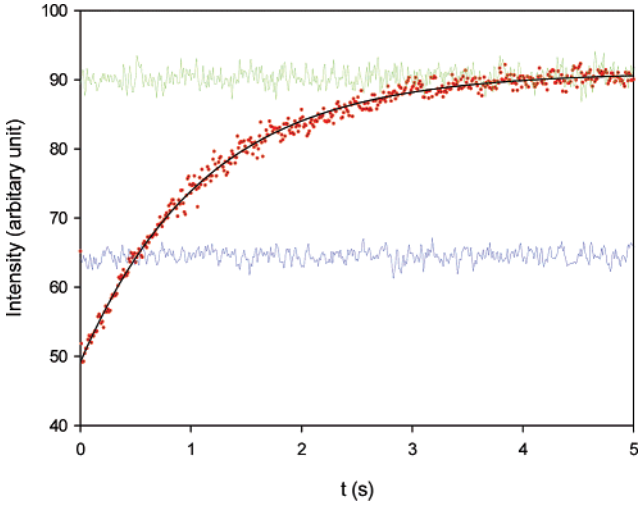

FIGURE 6: Fluorescence-monitored folding process of src SH3 at 4 °C in 50 mM PBS at pH 3.0 in the absence of 45% EGOH. Fluorescence was excited by 295 nm, and the integrated fluorescence above 325 nm was collected. The green line is the final level (refolded, measured 3 min after refolding). The blue line is the initial level (unfolded state). Red dots represent the monitored refolding trace. The black line is the simulated curve to a single exponential.

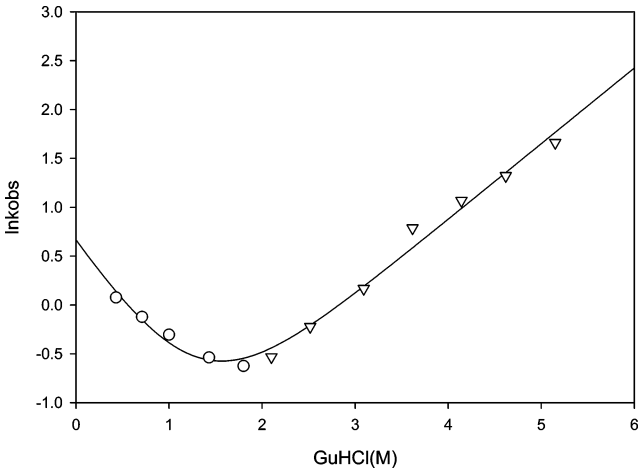

FIGURE 7: GuHCl dependence of ln(k_{obs}) at 4 °C in 50 mM PBS at pH 3.0. The solid line is the best fit from the equation ln(k_{obs}) = ln[k_{f,H_2O} exp(−m_f[GuHCl]/RT) + k_{u,H_2O} exp(m_u[GuHCl]/RT)] (*1*). The kinetic parameters in 0 M GuHCl were calculated on the basis of the equation and summarized in Table 1. Open circles represent the folding at low denaturant concentration, and open triangles represent unfolding at high denaturant concentration.

refolding reaction of src SH3 was measured by SF X-ray scattering at 4 °C in 50 mM PBS at pH 3.0. The final concentration of protein was 2 mg/mL. The scattering data were accumulated 100 times in order to get a good signal to noise ratio. Results are shown in Figure 8. Figure 8a shows the time-resolved I_0 (zero angle intensity), which is nearly constant through the refolding process, indicating that no significant association occurred in the folding process. Figure 8c shows the kinetic refolding curve of src SH3 in terms of radius of gyration (R_g). It also shows two phases: a burst phase and an observable phase. The R_g of the protein was dramatically decreased from 27 Å (R_g of the unfolded src SH3 in 5 M GuHCl) to 18.5 Å within the dead time of the SF. Then it changed to 14.7 ± 0.4 Å with a single exponential decay with a rate of 0.90 ± 0.04 s^{-1}. The final

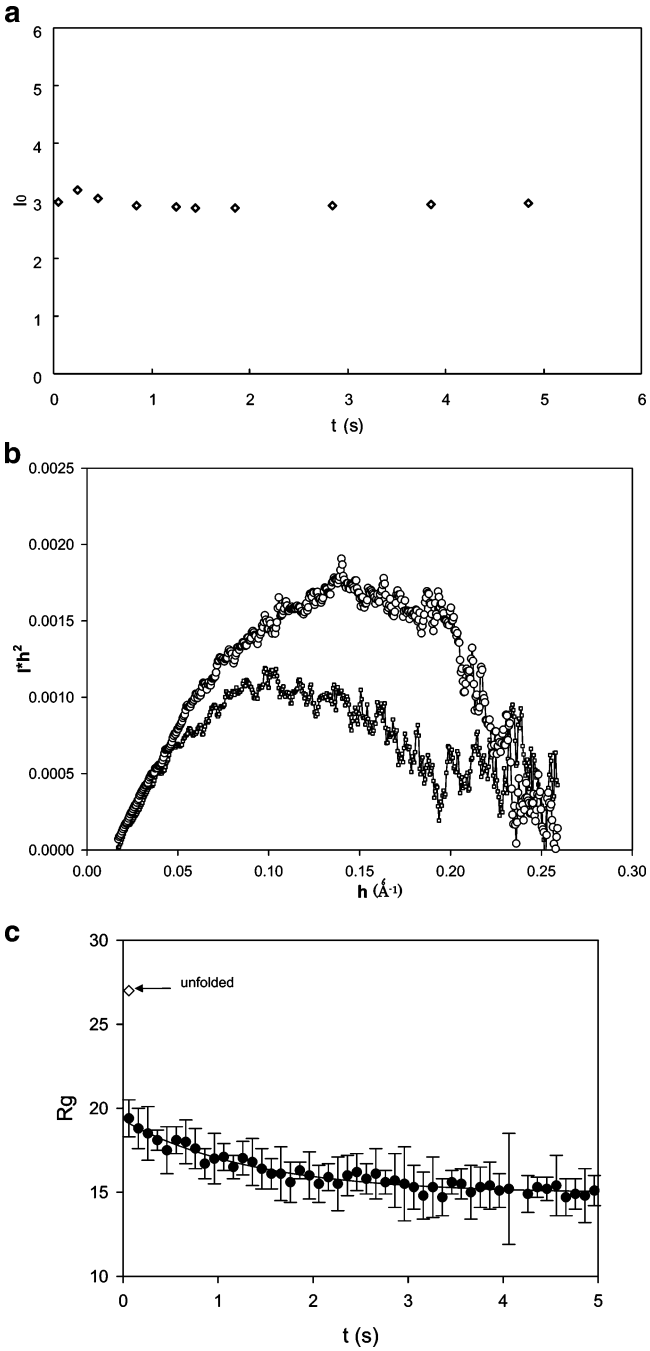

FIGURE 8: Time-resolved SAXS-monitored folding process of src SH3 at 4 °C in 50 mM PBS at pH 3.0. (a) Time course of zero angle intensity. The intensity did not change through the folding process within 5 s. It indicates the protein did not show aggregates during the process. (b) Kratky plots of src SH3 at 50 ms (open squares) and 5 s (open circles) after initiation of refolding by GuHCl concentration jump from 5 to 0.71 M. (c) Time-resolved radius of gyration (R_g). The burst phase and the observable phase can be clearly distinguished. The R_g was dramatically decreased from 27 to 18.5 Å within the dead time of the SF apparatus. The slow isomerization phase gave a rate constant of 0.90 ± 0.04 s^{-1}, accompanied with a further package of src SH3.

R_g value of the observable phase is in good agreement with that of the native state (14.6 Å).

The rate of 0.94 s^{-1} is similar with the result we observed from CD and fluorescence experiments (Table 2). Figure 8b shows the Kratky plot of the refolding process of src SH3. The src SH3 was already compact within the dead time of the SF apparatus, though it was different from the refolded

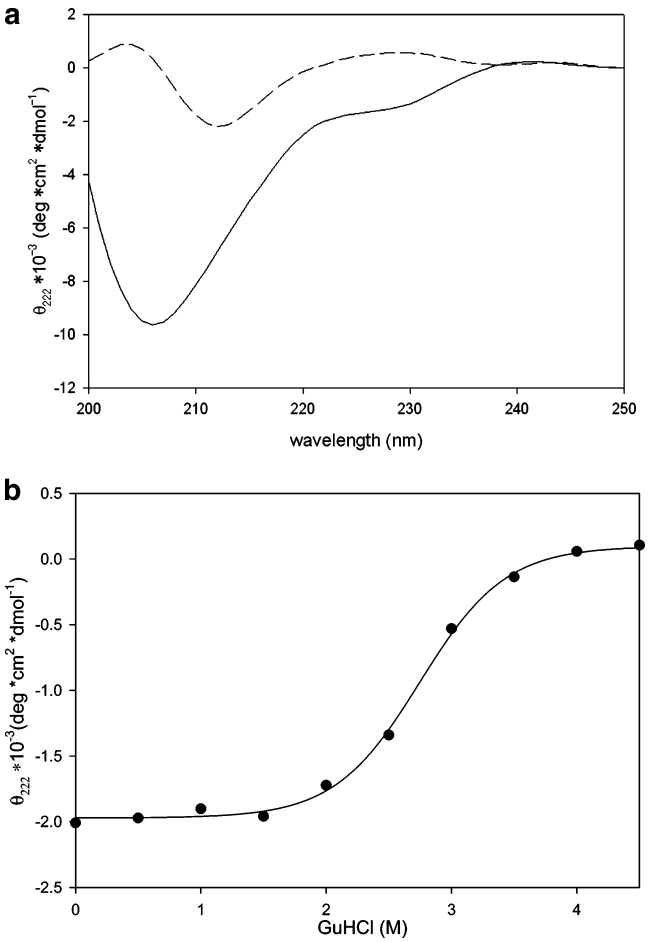

FIGURE 9: CD measurements of src SH3 in equilibrium in 50 mM PBS at pH 6.0. (a) CD spectra of the native and GuHCl-induced denatured src SH3 at 4 °C in 50 mM PBS at pH 6.0 (solid line, 0 M GuHCl; dashed line, 4.5 M GuHCl.) (b) Equilibrium GuHCl denaturation of src SH3 followed by CD at 4 °C. The CD signal was recorded at 222 nm. The curve is the fit to experimental data using the nonlinear least-squares method. The midpoint of denaturation is 2.76 M.

state (5 s later after mixing). Furthermore, the peak position of the intermediate Kratky curve appeared at the smaller angle than the refolded curve. This indicates that the compactness of the intermediate is not so tightly packed as the refolded one. R_g calculated from the peak of Kratky plots are 18.2 and 13.8 Å, in fairly good agreement with those estimated from Guinier analysis (*30*).

The kinetic data for all three kinds of probes can be fitted with a single exponential decay with an initial offset for the burst phase. The well-fitted signal gave similar rate constants. They are summarized in Table 2. The burst signal of the CD indicates that the intermediate has an α-helix-rich conformation.

Refolding of src SH3 at pH 6.0. We also performed the refolding experiments of src SH3 at physiological conditions, namely, in 50 mM PBS at pH 6.0 and 4 °C. As seen in Figure 10, a large overshoot burst phase is seen, suggesting that the α-helix-rich intermediate was formed within the dead time of the SF apparatus. The CD value changed from 500 to −6700 at the overshoot, and the slow isomerization process, corresponding to 56% of the signal, was accompanied with the decrease in α-helix content.

The kinetic fluorescence experiments were also performed at 4 °C, as shown in Figure 11. The burst and the single

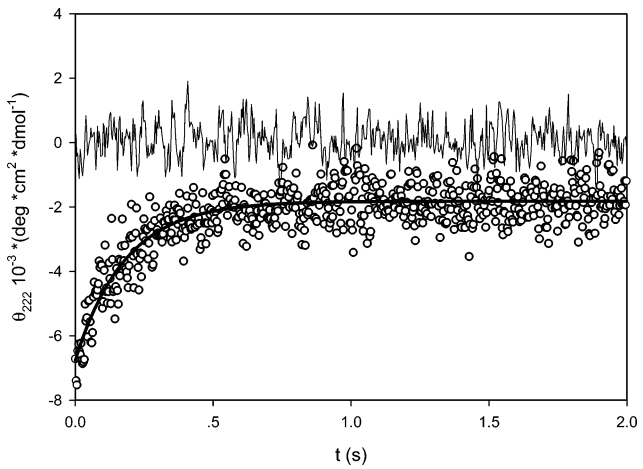

FIGURE 10: CD-monitored refolding process in 50 mM PBS at pH 6.0 at 4 °C from 5 to 0.71 M GuHCl.

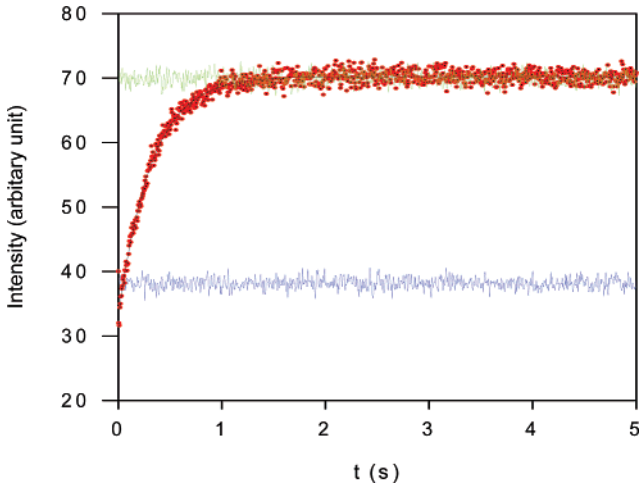

FIGURE 11: Fluorescence-monitored folding process of src SH3 at 4 °C in 50 mM PBS at pH 6.0. Fluorescence was excited at 295 nm, and integrated fluorescence was collected above 325 nm. The green line is the final level (refolded, measured 3 min after refolding). The blue line is the initial level (unfolded state). Red dots are the monitored refolding traces. The black line is the simulated curve to the single exponential.

exponential phase can be clearly distinguished. The experiment was also done at 20 °C, which also demonstrates the existence of the burst phase and the single exponential phase, though the folding rate at 20 °C is faster than at 4 °C. Obtained rate constants were summarized in Table 2, as were those obtained by kinetic CD. At 4 °C, the rate constant is similar to that of the kinetic CD. The folding rate constant at 20 °C is similar to other groups' results (*31*).

The kinetic results demonstrate that the α-helix-rich intermediates always appear and do not depend on the experimental conditions: pH, temperature, or the presence/absence of ethylene glycol.

Refolding of the src SH3 Homology Protein, Fyn SH3. The refolding experiment of Fyn SH3 was performed at 4 °C in 50 mM PBS at pH 6.0 in the absence of EGOH and at −20 °C in 50 mM PBS at pH 6.0 in the presence of antifreeze (45% EGOH). The measured CD results are shown in Figure 12. In both cases, we observed α-helix-rich intermediates on the folding pathway, as we did in the case of src SH3. The signal trace at 4 °C could be well fitted with a single exponential process. The CD overshot from

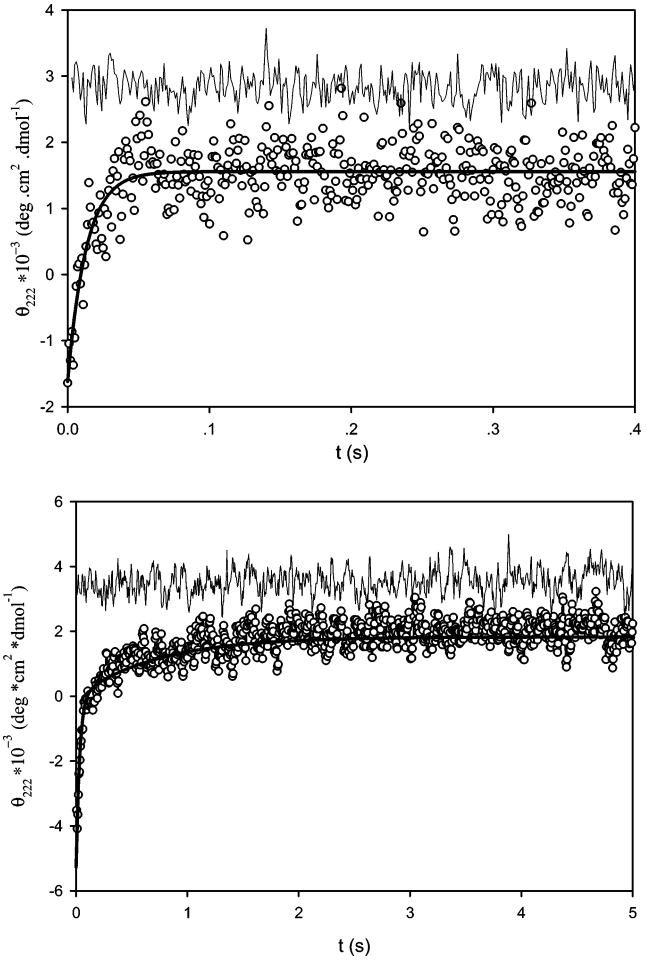

FIGURE 12: CD-monitored Fyn SH3 refolding. (a) The refolding process of Fyn SH3 at 4 °C in the absence of EGOH. The smoothed line represents a simulated kinetic curve as a single exponential, which gives a rate constant of 76 s^{-1}. (b) The kinetic refolding of Fyn SH3 at −20 °C in the presence of 45% EGOH as antifreeze. The black line is the refolding trace. The smoothed line shows the simulated one with a double exponential, which gives rate constants of 32 and 1.1 s^{-1}, respectively.

2200 to −4700 deg·cm^2·dmol^{-1}, and the slow isomerization process corresponds to 62% of the signal at 222 nm. However, the signal trace at −20 °C was fitted only with the double exponential process, of which the slow phase was 70 times slower than the phase observed at 4 °C. At −20 °C, the amplitude of the fast phase corresponds to about 26% of the signal changes, and the slow phase takes 48% signal changes. Interestingly, the amplitude of these two phases (observable phase at 4 °C and the slower phase at −20 °C) was nearly identical. This suggests that the slow phase obtained at −20 °C is corresponding to the phase obtained at 4 °C. The phase corresponding to the faster phase obtained at −20 °C was not observed at 4 °C. Probably the faster phase was too fast to be detected by the SF apparatus due to its dead time (6 ms). Obtained rate constants are shown in Table 2 in comparison with those of src SH3.

DISCUSSION

The Intermediate on the src SH3 Folding Pathway. One of the most important questions in protein folding is whether intermediates are formed or not. Recently, studies revealed that there are possible intermediates existing even in the case of small proteins. In this paper, we combined multiple probes to monitor the refolding process of src SH3. In CD experiments, we could observe an overshoot within the dead time of the SF (6 ms), both in the presence and in the absence of 45% EGOH. The amplitude did not change at various conditions, irrespective of the presence of EGOH. This demonstrates that the EGOH does not apparently affect the amplitude of the folding process of src SH3. This conclusion is consistent with our previous study on ubiquitin (*2*, *3*), where we combined experimental results and molecular dynamics to investigate the EGOH effect on protein folding. Both of them showed that EGOH did not influence the amplitude of the folding process, while the observable folding rate is slowed down in the presence of EGOH partly due to the increase of viscosity of the buffer. Actually, the folding rate was 30 times and 100 times slower at −10 and −20 °C than that at 4 °C.

To characterize the secondary structure of the intermediate, we plotted the amplitude of the burst phase at the wavelength region from 217 to 240 nm (Figure 5).

Is the CD Burst Due to α-Helix or Due to Aromatic Residues? It is notable that tryptophan, tyrosine, and the S−S bond also could make detectable CD signal changes at far-UV regions, during protein folding (*32*, *33*). As for S−S, src SH3 has no S−S bonds. Therefore, we cannot ascribe the observed burst to the S−S bond. src SH3 has four tyrosines and two tryptophans. These aromatic residues would give CD signal changes of at most 590 deg·cm^2·dmol^{-1} in the 220−230 nm region (*34*). In the present experiments, the burst amplitude is 2.6 × 10^3 deg·cm^2·dmol^{-1} even at 230 nm, much bigger than the value above. The burst signal is getting the largest at 222 nm but not at longer wavelength, indicating that the CD signal is mainly determined by the peptide bonds. Furthermore, the aromatic residues also give a CD signal in the near-UV region (*35*, *36*), while the SH3 burst shows nearly zero at 240 nm, which also confirms that the detected burst phase at lower wavelength is caused by secondary structure change. From these findings, we can conclude that the CD burst signal was mainly due to the secondary structure change, though the minor contributions from aromatic residues are not excluded.

The burst phase was also observed in kinetic fluorescence and X-ray solution scattering experiments. Rates of slow phases observed by the three methods are also in good agreement with each other. This indicates that the intermediate state was packed with the large amount of non-native α-helix.

We also performed fluorescence-SF with the same conditions as with SF-CD. The kinetic results were in good agreement. There is a clear intensity difference between the initial level and the starting level of the single exponential folding process. Although the experimental conditions were very different, the burst phase appeared at all conditions. Thus it is not due to the buffer conditions. We then propose the folding scheme of src SH3 as in Figure 13, where the unfolded src SH3 takes the compact α-helix-rich intermediate in its folding process.

Homologous Proteins Are Folded with a Similar Folding Pathway. In the present paper, we used the CD-SF to monitor the refolding process of another SH3 domain protein, Fyn SH3. src and Fyn SH3 domains have sequence homology as high as 73%. They share the same three-dimensional structure and folding topology (*37*). From the CD-SF result,

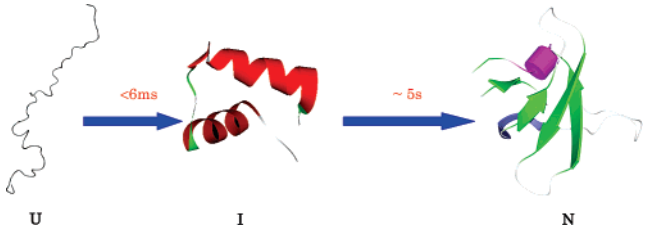

FIGURE 13: Proposed folding scheme of src SH3: U, unfolded state; I, intermediate; N, native state.

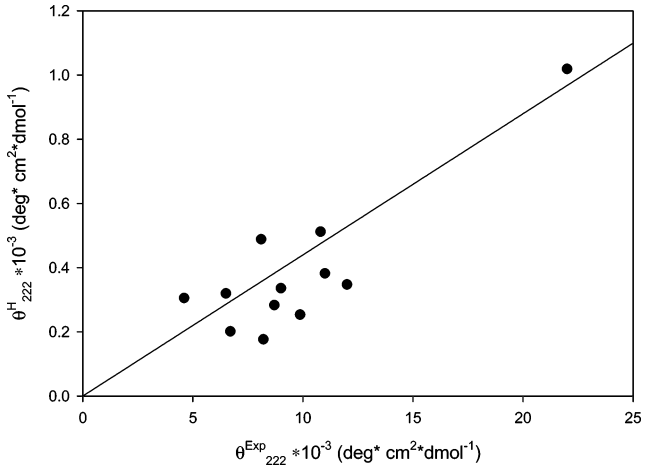

FIGURE 14: The calculated value of ellipticity at 222 nm by Helix2 (θ^{H}) versus the experimental value of ellipticity at 222 nm (θ^{exp}) of the α-helical burst for nine proteins. θ^{H} is calculated according to the equation $\theta = f(H)/100[-42500(1 - 4/N) - 640]$, where $f(H)$ is the fraction of helix calculated by Helix2 and N is the residual number. The correlation coefficient between θ^{H} and θ^{exp} was estimated as $r = 0.83$, demonstrating that the α-helix in the burst is strongly correlated to the helical fraction formed in equilibrium with a short lifetime.

it is clear that a similar helical burst phase appeared on the folding pathway of Fyn SH3. This indicates that Fyn SH3 also formed a non-native α-helix-rich intermediate in its folding pathway. Fyn SH3, however, showed another faster phase at −20 °C. This indicates that conversion of the α-helix to the native β-sheet takes two steps in the case of Fyn SH3.

Helical Structure Formation on the Refolding Process of the Protein. We have studied several proteins including α-helix-rich proteins [λ repressor (*38*), apomyoglobin (Matsumoto et al., unpublished)], β-structure-rich proteins [BLG (*4*), ELG (*39*), and ubiquitin (*3*)], and fully β-sheeted proteins (src SH3 and Fyn SH3). We have also measured some other α/β proteins [ribonuclease A (Li et al., unpublished) and lysozyme (Li et al., unpublished)]. In all cases, we found that folding goes through at least two steps: appearance of an α-helix-rich burst followed by a resolvable folding process to the native state.

To investigate the α-helical burst from another point of view, we have used several secondary structure prediction programs [PHD (*40*), Predator (*41*), SIMPA96 (*42*), GOV4 (*43*), ALB (*44*), AGADIR (*45*, *46*), and Helix2 (*47*)]. Results did not give a good correlation with the α-helical burst (correlation coefficients are less than 0.6) except Helix2, which gave a correlation coefficient of 0.83. Calculated θ_{222} (θ^{H}) by Helix2 is plotted against the α-helical burst (θ^{exp}) in Figure 14 and tabulated in Table 3. Some other data from refs *3*, *4*, *32*, *38*, and *48* are also shown in comparison. Although the calculated absolute amplitudes are roughly 20

Table 3: Experimentally Observed θ_{222} Values of the α-Helical Burst Amplitude and θ_{222} of the α-Helix Calculated by Helix2 for Nine Proteins[a]

protein	pH	burst amplitude ($\theta^{exp} \times 10^{-3}$)	calcd $\theta^{H} \times 10^{-3}$ by Helix2
horse heart apo Mb	6	9[b]	0.335
BLG	2	11[c]	0.382
ELG	4	6[d]	0.319
ELG	8.7	12[b]	0.347
Fyn SH3	6	8.7[e]	0.283
src SH3	3	8.2[e]	0.176
src SH3	6	6.7[e]	0.201
ubiquitin	5.9	9.8[f]	0.253
λ_{5-85}-repressor	7	22.0[d]	1.019
hen egg lysozyme	8	10.8,[g] 10.8[b]	0.511
hen egg lysozyme	2	8.1[b]	0.488
bovine ribonuclease A	8	4.3,[h] 4.6[b]	0.305

[a] Units of θ^{exp} and θ^{H} are deg·cm^2·dmol^{-1}. [b] Unpublished data. [c] Reference *4*. [d] Reference *38*. [e] The present work. [f] Reference *3*. [g] Reference *32*. This value is calculated with the assumption that the final value of Goldberg's experiment is the same with our measurement. [h] Reference *48*.

times smaller than the experimentally obtained θ_{222}, linearity between θ^{H} and θ^{exp} is fairly good. Helix2 implements the Lifson−Roig helix−coil transition theory incorporating the capping effects (*29*, *47*), while other many modern prediction programs were developed for predicting the native secondary structure with the use of empirical information including the tertiary structure from the Protein Data Bank. Actually, Helix2 is programmed only with the use of the interaction between the adjacent residues. These results might imply that the long-range interaction does not take a role in the early events of protein folding, and the local interaction takes dominant role in the early events of protein folding.

We thus propose that the initial event of protein folding is to form an α-helix due to a rapid helix−coil transition, and then some α-helices are stabilized by the interaction with each other. Such interaction leads to a compact state of the protein which can further reorganize to the native structure. Such intermediates are formed very rapidly.

The difference of the absolute θ value might indicate that α-helices formed in the early stage of folding are less stable, until they are collapsed to form more stable intermediates.

Compaction during src SH3 Refolding. The protein folding process is a complicated process, which involves thousands of weak bond formations and disruption. Hydrophobicity is one of the main forces to drive protein folding. Therefore, the time scale of hydrophobic collapse and correlation with secondary structure and tertiary structure formation is the most important question to be answered in protein folding.

X-ray solution scattering, combined with the rapid mixing technique, is a powerful tool to observe the conformational change of protein folding. There are several parameters used to describe the conformation of macromolecules in solution. The radius of gyration is a direct probe associated with molecular compaction.

It is notable that the large conformation changes in the structure of src SH3 were observed in all three probes: CD, fluorescence, and X-ray solution scattering. Good agreement of thermodynamic parameters indicates that the conformation changes, observed by different probes, took place simultaneously. Kinetic X-ray solution scattering shows a burst

phase similar to that of kinetic CD, in which the protein size dramatically decreased in 8.5 Å within the dead time of the SF (6 ms). The folding traces obtained by X-ray solution scattering, CD, and fluorescence at the same condition are well-fitted to the single exponential simulation with a nearly identical rate constant. It is reasonable that the helix burst is accompanied by the hydrophobicity-driven protein collapse. The Kratky plot of the first frame of the refolding process showed a peak, but not as high as the native state. This suggests that the protein was folded (at the intermediate state) but not as fully compact as the native state.

Thus, three probes lead to the conclusion that the less stable helix-rich compact intermediate was formed as a precursor of the native state. The slow phase was accompanied by the disruption of α-helical intermediates and the formation of the native conformation. The overshoot of fluorescence indicates that the native-like tryptophan package is accompanied with the disruption of the helix. This is in good agreement with our previous study on ubiquitin, where the compaction is associated with α-helix formation.

ACKNOWLEDGMENT

The X-ray solution scattering experiments were performed under proposal number 2004G184 of the Photon Factory. We also gratefully thank Prof. Masaki Kojima (Tokyo University of Pharmacy and Life Science), Prof. Martin Gruelele (University of Illinois), and Dr. Edgar Larios (University of Illinois) for valuable discussion, providing samples, or data analysis.

REFERENCES

1. Fersht, A. (1999) *Structure and Mechanism in Protein Science: A Guide to Enzyme Catalysis and Protein Folding*, W. H. Freeman, New York.
2. Qin, Z. J., Ervin, J., Larios, E., Gruebele, M., and Kihara, H. (2002) Formation of a compact structured ensemble without fluorescence signature early during ubiquitin folding, *J. Phys. Chem. 106*, 13040−13046.
3. Larios, E., Li, J. S., Schulten, K., Kihara, H., and Gruebele, M. (2004) Multiple probes reveal a native-like intermediate during low-temperature refolding of ubiquitin, *J. Mol. Biol. 340*, 115−125.
4. Qin, Z., Hu, D., Shimada, L., Nakagawa, T., Arai, M., Zhou, J. M., and Kihara, H. (2001) Refolding of beta-lactoglobulin studied by stopped-flow circular dichroism at subzero temperatures, *FEBS Lett. 507*, 299−302.
5. Kuwajima, K., Yamaya, H., Miwa, S., Sugai, S., and Nagamura, T. (1987) Rapid formation of secondary structure framework in protein folding studied by stopped-flow circular dichroism, *FEBS Lett. 221*, 115−118.
6. Kuwajima, K., Yamaya, H., and Sugai, S. (1996) The burst-phase intermediate in the refolding of beta-lactoglobulin studied by stopped-flow circular dichroism and absorption spectroscopy, *J. Mol. Biol. 264*, 806−822.
7. Hamada, D., Segawa, S., and Goto, Y. (1996) Non-native alpha-helical intermediate in the refolding of beta-lactoglobulin, a predominantly beta-sheet protein, *Nat. Struct. Biol. 3*, 868−873.
8. Hamada, D., and Goto, Y. (1997) The equilibrium intermediate of beta-lactoglobulin with non-native alpha-helical structure, *J. Mol. Biol. 269*, 479−487.
9. Shiraki, K., Nishikawa, K., and Goto, Y. (1995) Trifluoroethanol-induced stabilization of the alpha-helical structure of beta-lactoglobulin: implication for non-hierarchical protein folding, *J. Mol. Biol. 245*, 180−194.
10. Chikenji, G., and Kikuchi, M. (2000) What is the role of non-native intermediates of beta-lactoglobulin in protein folding?, *Proc. Natl. Acad. Sci. U.S.A. 97*, 14273−14277.
11. Musacchio, A., Gibson, T., Lehto, V. P., and Saraste, M. (1992) SH3−an abundant protein domain in search of a function, *FEBS Lett. 307*, 55−61.
12. Noble, M. E., Musacchio, A., Saraste, M., Courtneidge, S. A., and Wierenga, R. K. (1993) Crystal structure of the SH3 domain in human Fyn; comparison of the three-dimensional structures of SH3 domains in tyrosine kinases and spectrin, *EMBO J. 12*, 2617−2624.
13. Qin, Z. J., Vyas, S., Fink, A. L., Li, J. S., and Kihara, H. (2007) Transient α-helical structure during folding of Src SH3 domain at subzero temperatures. *J. Kansai Med. Univ.* (in press).
14. Chikenji, G., Fujitsuk, Y., and Takada, S. (2004) Protein folding mechanisms and energy landscape of src SH3 domain studied by a structure prediction toolbox, *Chem. Phys. 307*, 157−162.
15. Grantcharova, V. P., and Baker, D. (1997) Folding dynamics of the src SH3 domain, *Biochemistry 36*, 15685−15692.
16. Patton, W. F., Chung-Welch, N., Lopez, M. F., Cambria, R. P., Utterback, B. L., and Skea, W. M. (1991) Tris-tricine and Tris-borate buffer systems provide better estimates of human mesothelial cell intermediate filament protein molecular weights than the standard Tris-glycine system, *Anal. Biochem. 197*, 25−33.
17. Gill, S. C., and von Hippel, P. H. (1989) Calculation of protein extinction coefficients from amino acid sequence data, *Anal. Biochem. 182*, 319−326.
18. Saxena, V. P., and Wetlaufer, D. B. (1971) A new basis for interpreting the circular dichroic spectra of proteins, *Proc. Natl. Acad. Sci. U.S.A. 68*, 969−972.
19. Chen, Y. H., Yang, J. T., and Martinez, H. M. (1972) Determination of the secondary structures of proteins by circular dichroism and optical rotatory dispersion, *Biochemistry 11*, 4120−4131.
20. Amemiya, Y., Wakabayashi, K., Hamanaka, T., Wakabayashi, T., and Hashizume, H. (1983) Design of a small-angle X-ray diffractometer using synchrotron radiation at the photon factory, *Nucl. Instrum. Methods 208*, 471−477.
21. Amemiya, Y., Ito, K., Yagi, N., Asano, Y., Wakabayashi, K., Ueki, T., and Endo, T. (1995) Large-aperture TV detector with a beryllium-windowed image intensifier for X-ray diffraction, *Rev. Instrum. Methods 66*, 2290−2294.
22. Ito, K., Kamikubo, H., Arai, M., Kuwajima, K., Amemiya, Y., and Endo, T. (2001) Calibration method for contrast reduction problem in the X-ray image-intensifier, *Photon Factory Activity Rep. 18*, 275.
23. Ito, K., Kamikubo, H., Yagi, N., and Amemiya, Y. (2005) Correction method and software for image distortion and non-uniform response in charge-coupled device-based X-ray detectors utilizing X-ray image intensifier, *Jpn. J. Appl. Phys. 44*, 8684−8691.
24. Guinier, A., and Fournet, G. (1955) in *Small Angle Scattering of X-rays*, Wiley, New York.
25. Glatter, O., and Kratky, O. (1982) in *Small Angle X-ray Scattering*, Academic Press, London.
26. Kojima, M., Timchenko, A. A., Higo, J., Ito, K., Kihara, H., and Takahashi, K. (2004) Structural refinement by restrained molecular-dynamics algorithm with small-angle X-ray scattering constraints for a biomolecule, *J. Appl. Crystallogr. 37*, 103−109.
27. Provencher, S. W., and Glöckner, J. (1981) Estimation of globular protein secondary structure from circular dichroism, *Biochemistry 20*, 33−37.
28. Richardson, J. M., and Makhatadze, G. I. (2004) Temperature dependence of the thermodynamics of helix-coil transition, *J. Mol. Biol. 335*, 1029−1037.
29. Rohl, C. A., and Baldwin, R. L. (1998) Deciphering rules of helix stability in peptides, *Methods Enzymol. 295*, 1−26.
30. Semisotnov, G. V., Kihara, H., Kotova, V. N., Kimura, K., Amemiya, Y., Wakabayashi, K., Serdyuk, N. I., Timchenko, A. A., Chiba, K., Nikaido, K., Ikura, T., and Kuwajima, K. (1996) Protein globularization during folding. A study by synchrotron small-angle X-ray scattering, *J. Mol. Biol. 262*, 559−574.
31. Riddle, D. S., Grantcharova, V. P., Santiago, J. V., Alm, E., Ruczinski, I., and Baker, D. (1999) Experiment and theory highlight role of native state topology in SH3 folding, *Nat. Struct. Biol. 6*, 1016−1024.
32. Chaffotte, A. F., Guillou, Y., and Goldberg, M. E. (1992) Kinetic resolution of peptide bond and side chain far-UV circular dichroism during the folding of hen egg white lysozyme, *Biochemistry 31*, 9694−9702.

33. Radford, S. E., Dobson, C. M., and Evans, P. A. (1992) The folding of hen lysozyme involves partially structured intermediates and multiple pathways, *Nature 358*, 302−307.
34. Adler, A. J., Greenfield, N. J., and Fasman, G. D. (1973) Circular dichroism and optical rotatory dispersion of proteins and polypeptides, *Methods Enzymol. 27*, 675−735.
35. Woody, R. W. (1995) Circular dichroism, *Methods Enzymol. 246*, 34−71.
36. Woody, R. W. (2004) Circular dichroism of protein-folding intermediates, *Methods Enzymol. 380*, 242−285.
37. Northey, J. G., Di Nardo, A. A., and Davidson, A. R. (2002) Hydrophobic core packing in the SH3 domain folding transition state, *Nat. Struct. Biol. 9*, 126−130.
38. Dumont, C., Matsumura, Y., Kim, S. J., Li, J. S., Kondrashkina, E., Kihara, H., and Gruebele, M. (2007) Solvent-tuning the collapse and secondary structure formation of λ_{6-85}, *Protein Sci*. (in press).
39. Fujiwara, K., Arai, M., Shimizu, A., Ikeguchi, M., Kuwajima, K., and Sugai, S. (1999) Folding-unfolding equilibrium and kinetics of equine beta-lactoglobulin: equivalence between the equilibrium molten globule state and a burst-phase folding intermediate, *Biochemistry 38*, 4455−4463.
40. Rost, B., and Sander, C. (1994) Combining evolutionary information and neural networks to predict protein secondary structure, *Proteins 19*, 55−72.
41. Frishman, D., and Argos, P. (1996) Incorporation of non-local interactions in protein secondary structure prediction from the amino acid sequence, *Protein Eng. 9*, 133−142.
42. Levin, J. (1997) Exploring the limits of nearest neighbor secondary structure prediction, *Protein Eng. 7*, 771−776.
43. Garnier, J., Gibrat, J. F., and Robson, B. (1996) GOR secondary structure prediction method version IV, *Methods Enzymol. 266*, 540−553.
44. Ptitsyn, O. B., and Finkelstein, A. V. (1983) Theory of protein secondary structure and algorithm of its prediction, *Biopolymers 22*, 15−25.
45. Munoz, V., and Serrano, L. (1995) Elucidating the folding problem of helical peptides using empirical parameters. II. Helix macrodipole effects and rational modification of the helical content of natural peptides, *J. Mol. Biol. 245*, 275−296.
46. Munoz, V., and Serrano, L. (1995) Elucidating the folding problem of helical peptides using empirical parameters. III. Temperature and pH dependence, *J. Mol. Biol. 245*, 297−308.
47. Rohl, C. A., Chakrabartty, A., and Baldwin, R. L. (1996) Helix propagation and N-cap propensities of the amino acids measured in alanine-based peptides in 40 volume percent trifluoroethanol, *Protein Sci. 5*, 2623−2637.
48. Kimura, T., Akiyama, S., Uzawa, T., Ishimori, K., Morishima, I., Fujisawa, T., and Takahashi, S. (2005) Specifically collapsed intermediate in the early stage of the folding of ribonuclease A, *J. Mol. Biol. 350*, 349−362.

BI0618262